SYNTHESIS, SPECTROSCOPY AND SPECTROELECTROCHEMISTRY OF CHLOROCARBONYL {1,2-BIS[(2,6-DIISOPROPYLPHENYL)IMINO]-ACENAPHTHENE-κ²-*N,N*}RHODIUM(I)

Taasje MAHABIERSING[1], Henk LUYTEN[2], Ronald C. NIEUWENDAM[3] and František HARTL[4],*

Institute of Molecular Chemistry, Universiteit van Amsterdam, Nieuwe Achtergracht 166, 1018 WV Amsterdam, The Netherlands; e-mail: [1] taasje@science.uva.nl, [2] luyten@science.uva.nl, [3] rnieuwen@science.uva.nl, [4] hartl@science.uva.nl

*Dedicated to Professor Sergio Roffia (**Università** di Bologna) for his outstanding record in the field of electrochemistry.*

Reaction of the dinuclear complex [{Rh(CO)₂}₂(μ-Cl)₂] with an α-diimine ligand, 1,2-bis[(2,6-diisopropylphenyl)imino]acenaphthene (*i*Pr₂Ph-bian), produces square-planar [RhCl(CO)(*i*Pr₂Ph-bian)]. For the first time, 2:1 and 1:1 α-diimine/dimer reactions yielded the same product. The rigidity of *i*Pr₂Ph-bian together with its flexible electronic properties and steric requirements of the 2,6-diisopropyl substituents on the benzene rings allow rapid closure of a chelate bond and replacement of a CO ligand instead of chloride. A resonance Raman study of [RhCl(CO)(*i*Pr₂Ph-bian)] has revealed a predominant Rh-to-bian charge transfer (MLCT) character of electronic transitions in the visible spectral region. The stabilisation of [RhCl(CO)(*i*Pr₂Ph-bian)] in lower oxidation states by the π-acceptor *i*Pr₂Ph-bian ligand was investigated *in situ* by UV-VIS, IR and EPR spectroelectrochemistry at variable temperatures. The construction of the novel UV-VIS-NIR-IR low-temperature OTTLE cell used in these studies is described in the last part of the paper.
Keywords: Electrochemistry; Reduction; Rhodium; α-Diimine; Spectroelectrochemistry; Infrared spectroscopy; Electron paramagnetic resonance; Resonance Raman.

During the last three decades numerous rhodium complexes with bidentate nitrogen ligands have been synthesized[1]. The gradually increasing interest in these complexes stems from their catalytic activity in several processes such as hydroformylation[2], hydrosilylation[3], hydrogenation[4] and hydrogen transfer reactions[4] (*e.g.* selective reduction of nitroaromatics to amines). They also exhibit biological activitity[1h] and act as catalysts in electrochemical reduction and activation of carbon dioxide[1h,5]. Square-planar d⁸ Rh(I) complexes may form linear stacks[1e,6] as a basis for novel anisotropic materi-

als, depending on the steric properties of the (aromatic) nitrogen chelate that control the strength of metal–metal interactions.

Capable of undergoing facile oxidative addition[1a], square-planar complexes [RhCl(CO)(α-diimine)] serve as precursors of pseudooctahedral Rh(III) species, *e.g.* photoreactive [Rh(CO)(R)$_2$(dmb)] (R = Me, *i*Pr; dmb = 4,4′-dimethyl-2,2′-bipyridine)[7], or the hydrosilylation catalyst [RhClH(SiR′$_3$)-(R-dab)] (R-dab = 1,2-bis(alkylimino)ethane)[3]. Their syntheses usually start from the dinuclear complex [{Rh(CO)$_2$}$_2$(μ-Cl)$_2$]. Its reaction with two molar equivalents of α-diimine (1:1 metal/ligand stoichiometry) has been found to produce the mononuclear square-planar complexes [RhCl(CO)(α-diimine)]: α-diimine = *e.g.* 2,2′-bipyridine (bpy)[1a,1i,6], pyridine-2-carbaldehyde imines (R-pyca)[1a] and a number of R-dab ligands[3]. Five-coordinate complexes [RhCl(CO)$_2$(μ-diimine)], in equilibrium with four-coordinate cation [Rh(CO)$_2$(α-diimine)]Cl (dependent on the solvent polarity) have also been reported[1h,8,9]. On the other hand, if reacted in equimolar amounts (2:1 metal/ligand stoichiometry), the R-dab ligand may coordinate in dinuclear complexes, forming a σ,σ′-*N*,*N*-bridge between two {RhCl(CO)$_2$} units[10,11], or in ionic species [Rh(CO)$_2$(R-dab)]$^+$[RhCl$_2$(CO)$_2$]$^-$ (refs[10,12]). The latter type of products has also been reported for chelating aromatic bpy[13] and 1,10-phenanthroline (phen)[1h] ligands. The same qualitative conclusions can be drawn for the dinuclear precursor [{RhCl(cod)}$_2$] (cod = cycloocta-1,5-diene)[14].

In this paper we report the reaction of [{Rh(CO)$_2$}$_2$(μ-Cl)$_2$] with a rigid analogue of Ar-dab (Ar = aryl) ligands, *viz.* 1,2-bis[(2,6-diisopropylphenyl)-imino]acenaphthene (*i*Pr$_2$Ph-bian; Fig. 1) in the 1:1 and 2:1 Rh/(*i*Pr$_2$Ph-bian) stoichiometry. The Ar-bian ligands with a rigid naphthalene backbone bridging two C=N imine functions in a fixed cis orientation favour bidentate (chelating) over monodentate coordination. They have been
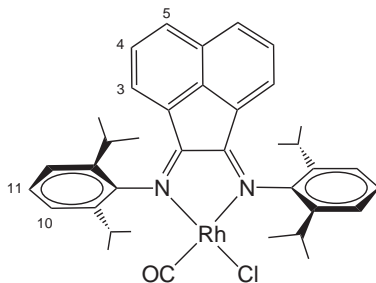

F$_{IG}$. 1
Schematic molecular structure of the [RhCl(CO)(*i*Pr$_2$Ph-bian)] complex with proton numbering

shown by van Asselt *et al.* to have a pronounced effect on the stability of a number of organopalladium(IV) and organoplatinum(IV) complexes due to their good σ-donor capacity and a limited tendency to undergo dissociation of a coordinated N atom[15]. Even in zero-valent palladium and platinum complexes [M(alkene)(Ar-bian)] the Ar-bian ligand still acts as a σ-donor, the metal-to-alkene π-back-bonding being the major factor for the stability of these complexes[16]. At the same time, the closely related Ar-dab ligands act as good π-acceptors capable of stabilising a metal–halide bond in low oxidation states[17]. We were interested whether this special (flexible) character of the *i*Pr$_2$Ph-bian-to-metal bonding (rigidity, σ-donor and π-acceptor capacity, steric requirements of the 2,6-diisopropylphenyl groups, in particular at the vacant axial coordination sites of a square-planar complex) would have any notable effect on the reaction with [{Rh(CO)$_2$}$_2$(μ-Cl)$_2$].

In the second part, after spectroscopic characterisation, we have undertaken a spectroelectrochemical study of the single reaction product, [RhCl(CO)(*i*Pr$_2$Ph-bian)], in order to examine the stabilising coordination of *i*Pr$_2$Ph-bian in the lower oxidation states of the complex. This study was performed with an improved version of previously described[18] optically transparent thin-layer electrochemical (OTTLE) cell suited for *in situ* UV-VIS-NIR-IR experiments at variable temperatures. The cell is depicted and described in the last part of this work.

EXPERIMENTAL

Materials and Preparations

Tetrahydrofuran (THF), dichloromethane (DCM), hexane and butyronitrile (PrCN), all analytical grade (Acros), were dried using Na/benzophenone (THF, hexane) and CaH$_2$ (DCM, PrCN), and distilled *prior* to use under an atmosphere of dry nitrogen. Tetrabutylammonium hexafluorophosphate (TBAH; Aldrich) was recrystallised twice from absolute ethanol and dried *prior* to use under vacuum at 80 °C for 10 h. Ferrocene (Fc; Schuchardt) and tetrabutylammonium chloride (Acros) were used as received. All reactions were carried out and electrochemical samples were prepared under an atmosphere of dry nitrogen, using standard Schlenk techniques. Column chromatography was performed on pre-dried and activated silica gel (Merck, 60 mesh). The ligand 1,2-bis[(2,6-diisopropylphenyl)imino]acenaphthene (*i*Pr$_2$Ph-bian) was prepared by a published procedure[19]. The precursor complex [{Rh(CO)$_2$}$_2$(μ-Cl)$_2$] was purchased from Degussa.

Synthesis of [RhCl(CO)(*i*Pr$_2$-bian)]

The ligand *i*Pr$_2$Ph-bian (50 mg, 10^{-4} mol) was added at room temperature to a stirred solution of [{Rh(CO)$_2$}$_2$(μ-Cl)$_2$] (19.4 mg, 5×10^{-5} mol) in DCM. The solution colour turned immediately dark green. The solvent was evaporated under vacuum and the crude product was

purified by column chromatography on silica gel with hexane/DCM (1:3 v/v) as the eluent. Yield 90%. Dark green crystals were obtained by slow evaporation of an acetone solution of the complex in the air. The crystal structure of the square-planar complex (low-symmetry orthorhombic microcrystals, space group *Pbca*) was determined from high-resolution synchrotron X-ray powder diffraction data, as described in detail elsewhere[20]. Results of a single-crystal X-ray diffraction study will be reported in another publication, together with data for a related Rh(III) species[21]. Here we note that the complex [RhCl(CO)(*i*Pr$_2$Ph-bian)] crystallised with one solvent (acetone) molecule and the single crystals were tetragonal with space group *I*4$_1$/*a*. The complex [RhCl(CO)(*i*Pr$_2$Ph-bian)] is non-conducting in acetone, DCM and methanol, in agreement with a strong Rh–Cl bond.

^{1}H NMR (CDCl$_3$, see Fig. 1 for the proton numbering): 0.96 (d, 6 H, CH$_3$ (*i*Pr)); 0.99 (d, 6 H, CH$_3$ (*i*Pr)); 1.43 (d, 6 H, CH$_3$ (*i*Pr)); 1.48 (d, 6 H, CH$_3$ (*i*Pr)); 3.54 (sept, 2 H, CH (*i*Pr)); 3.65 (sept, 2 H, CH (*i*Pr)); 6.47 (d, 1 H, H$_3$); 6.62 (d, 1 H, H$_{3'}$); 7.28–7.53 (m, 8 H, H$_{4,10,11}$); 8.03 (d, 1 H, H$_5$); 8.07 (d, 1 H, H$_{5'}$). ^{13}C NMR (CDCl$_3$): 186 (d, CO, ^2J(Rh-C) = 79). IR (neat CH$_2$Cl$_2$): 1998 cm^{-1}. MS FD$^+$, *m/z*: 666 [M$^+$]. For C$_{37}$H$_{40}$ClN$_2$ORh (666.5) calculated: 66.6% C, 6.0% H, 4.2% N; found: 66.4% C, 6.1% H, 4.1% N.

Notably, the same exclusive product, green [RhCl(CO)(*i*Pr$_2$Ph-bian)], was rapidly formed under identical reaction conditions, but using only half amount of *i*Pr$_2$Ph-bian (50 mg, 10^{-4} mol), *i.e.*, equimolar with [{Rh(CO)$_2$}$_2$(μ-Cl)$_2$]. It was separated from the reaction mixture by column chromatography, purified and characterised as described above. The IR spectrum of the reaction mixture did not indicate the presence of any dicarbonyl species containing the {Rh(CO)$_2$(*i*Pr$_2$Ph-bian)}$^+$ moiety.

Techniques

IR spectra were recorded with a Bio-Rad FTS-7 spectrometer, UV-VIS spectra with a software-updated Perkin–Elmer Lambda 5 spectrophotometer, NMR spectra with a Bruker AMX 300 spectrometer (δ, ppm; *J*, Hz), EPR spectra with a Varian Century E-104A X-band spectrometer, and mass spectra (FAB$^+$) with a JEOL JMS SX/SX102A four-sector mass spectrometer equipped with a fast atom bombardment source. EPR spectra were simulated with PEST Winsim (version 0.96)[22]. Elemental analysis data were obtained from an Elemental Vario EL apparatus (Foss Electric). Resonance Raman (rR) spectroscopic measurements were performed with a Dilor XY spectrometer, equipped with a Wright Instruments CCD detector. A Spectra Physics 2040E argon-ion laser in combination with Coherent model CR490 and Coherent CR590 dye lasers (employing Coumarin 6 and Rhodamine 6G dyes, respectively) served as excitation sources under a 180° back-scattering geometry. Data acquisition was controlled by Dilor Labspec 2.08 software. Wavenumbers of Raman bands were calibrated with respect to KNO$_3$, employed as the material for pellets containing the studied compound.

Electrochemistry and Spectroelectrochemistry

Cyclic voltammetric measurements were performed with an EG&G PAR 283 potentiostat. Cyclic voltammograms were recorded with a home-made air-tight voltammetric cell. The electrode set consisted of a platinum disk working electrode (apparent surface area of 0.42 mm^2), polished carefully with a 0.25 μm diamond paste (Oberflächentechnologien Ziesmer, Kempen, Germany), a Pt-gauze auxiliary electrode and a Ag-wire pseudoreference electrode. The standard ferrocene/ferrocenium (Fc/Fc$^+$) redox couple served as internal reference system[23]. Conversion of the Fc/Fc$^+$ potential scale to other reference systems can be

found elsewhere[24]. IR and UV-VIS spectroelectrochemical experiments at variable temperatures were conducted with an optically transparent thin-layer electrochemical cell depicted and described in detail in this work. EPR spectroelectrochemical experiments at low temperatures were carried out with an air-tight three-electrode version of the Allendoerfer-type cell equipped with Au-helix working, Pt-helix auxiliary and Ag-wire pseudoreference electrodes[25]. The spectroelectrochemical samples typically contained 10^{-4} M (EPR) or 10^{-3} M (UV-VIS) or 3×10^{-3} M (IR) rhodium complex and 3×10^{-1} M supporting electrolyte. The potential of the working electrode was controlled by a PA4 (EKOM, Czech Republic) potentiostat. Electrical conductivity measurements were performed with a Consort K720 digital conductometer (Salm & Kipp, Breukelen, The Netherlands) equipped with a Philips PW 9510 Pt electrode.

RESULTS AND DISCUSSION

Synthesis and Characterisation of [RhCl(CO)(iPr₂Ph-bian)]

The complex [RhCl(CO)(*i*Pr₂Ph-bian)] was prepared in high yield from the dinuclear precursor [{Rh(CO)₂}₂(μ-Cl)₂] and the *i*Pr₂Ph-bian ligand. Independently of the Rh/(*i*Pr₂Ph-bian) ratio used, *viz.* 1:1 and 2:1, only exclusive formation of [RhCl(CO)(*i*Pr₂Ph-bian)] was observed. This is for the first time that the 2:1 reaction yields the neutral square-planar complex, in contrast to reactant ratio-, solvent-, ligand- and temperature-dependent reaction routes and equilibria established for other bidentate α-diimine ligands (phen, bpy, R-pyCa, R-dab). This result is ascribed to the extraordinary properties of the *i*Pr₂Ph-bian ligand, in particular to its rigid backbone promoting rapid closure of a chelate ring. Besides the chelating capability of *i*Pr₂Ph-bian, also electronic (and steric) properties are important, which can be finely tuned by varying substituents on the benzene rings. Thus, the substitution of one of the CO ligands in [{Rh(CO)₂}₂(μ-Cl)₂] is facile with the 2,6-diisopropylphenyl substituents (*i*Pr₂Ph-bian). The same (so far unpublished) result has also been obtained for 2,6-dimethylphenyl substituents (Me₂Ph-bian). On the contrary, the reactions of [{Rh(CO)₂}₂(μ-Cl)₂] with less donating and sterically less demanding Ar-bian ligands having 4-methoxyphenyl (MeOPh-bian), *p*-tolyl (MePh-bian) or unsubstituted phenyl (Ph-bian) groups on the imine nitrogen, are significantly less efficient. In fact, in the latter cases the reactions can only be promoted by addition of the decarbonylating agent Me₃NO into the solution. According to the literature, the coordination of α-diimine to [{Rh(CO)₂}₂(μ-Cl)₂] produces five-coordinate [RhCl(CO)₂(α-diimine)] *prior* to the chloride- or CO-loss steps[1m]. For Ar-bian ligands, the Rh–Cl bond can be strongly stabilised by the presence of the strongly bound π-acceptor chelate, pushing out one of the car-

bonyls independently of the Rh/(Ar-bian) ratio. The CO dissociation from the sterically congested axial position in the tentative square-pyramidal transient then becomes facilitated by the steric crowding due to 2,6-di-substitution of the benzene rings.

The crystal structure determinations[20,21] have confirmed the square-planar geometry of [RhCl(CO)(iPr$_2$Ph-bian)] with Cl$^-$ present in the rhodium coordination sphere. The chloride ligand remains firmly coordinated even in ethanol, as was shown by the conductivity measurements. Also ^{1}H NMR spectra clearly prove the asymmetric environment of the iPr$_2$Ph-bian ligand, which would not be the case if ionic complexes [Rh(CO)$_2$(iPr$_2$Ph-bian)]Cl or [Rh(CO)$_2$(iPr$_2$Ph-bian)]$^+$[RhCl$_2$(CO)$_2$]$^-$ were formed. The IR CO-stretching frequency of [RhCl(CO)(iPr$_2$Ph-bian)] (Table I) is much higher than those of [RhCl(CO)(dmb)] (dmb = 4,4′-dimethyl-2,2′-bipyridine; 1970 cm^{-1} in THF) and [RhCl(CO)(bpy)] (bpy = 2,2′-bipyridine; 1977 cm^{-1} in MeCN). This difference agrees with the large π-acceptor capacity of the iPr$_2$Ph-bian ligand and limited π-back-donation towards the carbonyl. Green [RhCl(CO)(iPr$_2$Ph-bian)] exhibits in the visible region two intense absorption bands with solvent-dependent absorption maxima around 450 and 650–670 nm (Fig. 2). The solvatochromism suggests a predominant (Cl)Rh-to-iPr$_2$Ph-bian charge-transfer character of the corresponding electronic transitions. Convincing evidence for this assignment has been provided by resonance Raman spectroscopy that enables identification of the particular vibrational modes of the complex coupled to the allowed electronic excitation.
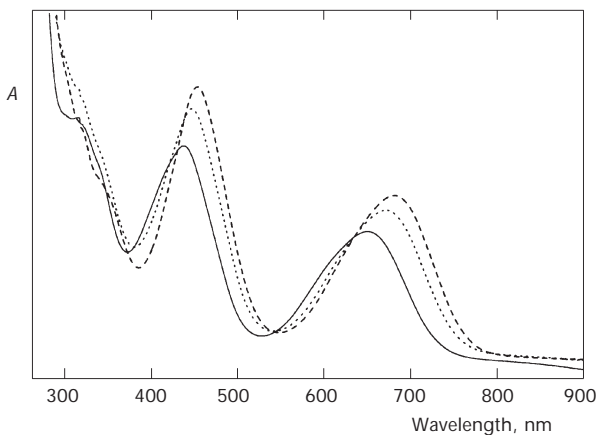

FIG. 2
UV-VIS spectra of [RhCl(CO)(iPr$_2$Ph-bian)], showing the solvatochromic absorption bands in the visible region. Solvents: PrCN (full line), THF (dotted line), benzene (dashed line)

Resonance Raman Spectra of [RhCl(CO)(iPr$_2$Ph-bian)]

Raman spectra of the title complex dispersed in a KNO$_3$ pellet were recorded at several excitation wavelengths directed into the two lowest absorption bands (λ_{max} = 453 and 688 nm, KBr pellet): 458.5, 488, 514.5 and 547 nm (band I); 582, 591, 611 and 638 nm (band II). Representative spectra are shown in Fig. 3. Most importantly, irradiation at wavelengths of both absorption bands causes resonant enhancement of Raman intensities for the modes at 1988 and 1541 cm^{-1}, which can be assigned safely as the ν(CO) and *i*Pr$_2$Ph-bian ν_s(CN) vibrations, respectively[26]. Also other Raman bands belong to internal vibrational modes of the *i*Pr$_2$Ph-bian ligand[26,27]: 1613 and 1602 cm^{-1}, Ph-ring, ν(C–C); 1195 and 1149 cm^{-1}, Ph-ring C–H deformation; 962 cm^{-1}, NCCN and/or Ph-ring deformation; 627 w cm^{-1}, Ph-ring (and/or MCO) deformation. It is noteworthy that the 1602 cm^{-1} mode only appears upon irradiation into the higher-lying band, whereas the 1613 cm^{-1} mode becomes enhanced upon the low-energy excitation. The intense Raman band at 489 cm^{-1} grows together with the 1613 cm^{-1} band; the corresponding vibration is tentatively assigned to ν(Rh–N) coupled to other, stretching or torsion modes of the RhC(O) or NCCN moieties[28].

The resonance enhancement of the CO-stretching mode in all the recorded resonance Raman spectra implies that the electron density at the Rh centre and the extent of the Rh-to-CO π-back-bonding are affected by the
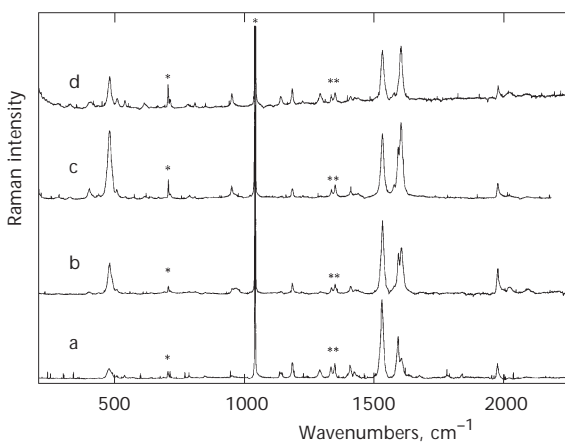

Fig. 3

Resonance Raman spectra of [RhCl(CO)(*i*Pr$_2$Ph-bian)] dispersed in a KNO$_3$ pellet. The KNO$_3$ bands are indicated by asterisks. Excitation wavelengths: a 458.5 nm (Ar$^+$ laser line); b 488 nm (Ar$^+$ laser line); c 514.5 nm (Ar$^+$ laser line); d 611 nm (Rhodamine 6G dye)

diverse electronic transitions underlying the two absorption bands in the visible spectral region; the involvement of iPr$_2$Ph-bian is indicated by the observation of the intensity enhancement for the ligand internal modes, in particular the ν(CN) vibration. The electronic transitions, consistent with their solvatochromism (see Fig. 1), therefore have acquired a predominant metal-to-ligand charge transfer (MLCT) character: the LUMO and other, higher-lying unoccupied orbitals of the complex are largely localized on the π^*(iPr$_2$Ph-bian) system (substituted Ph rings, the bian backbone), while the high-lying occupied molecular orbitals of [RhCl(CO)(iPr$_2$Ph-bian)] reside mainly on the Rh(CO,Cl) moiety.

Spectroelectrochemical Study of [RhCl(CO)(iPr$_2$Ph-bian)]

The reduction path of the title complex was studied in several solvents at variable temperatures by cyclic voltammetry and different spectroelectro-chemical techniques (IR, UV-VIS, EPR). The cyclic voltammetric data and IR CO-stretching wavenumbers of [RhCl(CO)(iPr$_2$Ph-bian)] and its reduction products are reported in Table I.

Cyclic voltammetry. The cyclic voltammogram of [RhCl(CO)(iPr$_2$Ph-bian)] in non-coordinating DCM shows an irreversible anodic step that was not studied in detail. In the cathodic region the reversible wave at –1.32 V, re-corded at 293 K and v = 100 mV s^{-1}, testifies to a high stability of the corre-sponding primary reduction product, the radical anion [RhCl(CO)(iPr$_2$Ph-bian)]$^{\bullet-}$. This result is not surprising, taking into account the localisation of the electron transfer on the strongly electron-withdrawing iPr$_2$Ph-bian ligand. In THF, the reversibility of the first cathodic process is preserved. The subsequent reduction of [RhCl(CO)(iPr$_2$Ph-bian)]$^{\bullet-}$ to the corresponding dianionic complex at –2.31 V is also fully reversible in this solvent. In sharp contrast to DCM and THF, in strongly coordinating butyronitrile (PrCN) the reversible behaviour on the time scale defined by v = 100 mV s^{-1} is ob-served only at T = 218 K (Fig. 4a). At room temperature, the first cathodic step is completely chemically irreversible, as testified by the absence of anodic counter-peak on the reverse scan (Fig. 4b). More negatively, a new reversible redox couple appears at –1.83 V. The positive potential shift com-pared to the reduction of [RhCl(CO)(iPr$_2$Ph-bian)]$^{\bullet-}$ in THF points to the replacement of the chloride ligand by a solvent molecule and to the reduc-tion of the radical complex [Rh(CO)(PrCN)(iPr$_2$Ph-bian)]$^{\bullet}$. In the reverse voltammetric scan this radical is oxidised at –0.94 V. This assignment of the electrode processes is shown below to be in full agreement with results of spectroelectrochemical studies. In order to demonstrate the influence of

PrCN on the reversibility of the one-electron electrochemical reduction of [RhCl(CO)(*i*Pr$_2$Ph-bian)], the cyclic voltammograms were also recorded in 30:1 (v/v) and 5:1 (v/v) DCM/PrCN (Fig. 5). In the former case the reduction is still partly chemically reversible and oxidations of both [RhCl(CO)-(*i*Pr$_2$Ph-bian)]$^{•-}$ and [Rh(CO)(PrCN)(*i*Pr$_2$Ph-bian)]$^{•}$ are observed on the reverse anodic scan beyond the cathodic wave of [RhCl(CO)(*i*Pr$_2$Ph-bian)]. In the latter case the reduction becomes totally irreversible, comparably with the behaviour in neat PrCN.

TABLE I
Electrode potentials and CO-stretching frequencies of the title complex [RhCl(CO)(*i*Pr$_2$-bian)] and species generated upon its electrochemical reduction in various media

Complex	Solvent	T, K	$E_{p,a}^{ox}$, V	$E_{1/2}^{red}$, V	$\nu(CO)$, cm^{-1}
[RhCl(CO)(*i*Pr$_2$Ph-bian)]	DCM	293	0.63[a]	–1.32	1998
	THF	293	0.62[a]	–1.25	1996
	PrCN	293	0.48[a,b]	–1.25[a]	1991
		218		–1.17	1989
		193			1988
[RhCl(CO)(*i*Pr$_2$Ph-bian)]$^{•-}$	THF	293		–2.31	1932
	PrCN	293			1930[c]
		218		–2.11	1929
		193			1927
[RhCl(CO)(*i*Pr$_2$Ph-bian)]$^{2-}$	PrCN	293			1872[c]
		218			1867
		193			1869
[RhCl(CO)(PrCN)(*i*Pr$_2$Ph-bian)]$^{•}$	PrCN	293	–0.94[d]	–1.83	1968
		218			1966
[RhCl(CO)(PrCN)(*i*Pr$_2$Ph-bian)]$^{-}$	PrCN	293			1904
		218			1904

[a] Chemically totally irreversible redox reaction. [b] In 5:1 (v/v) PrCN/DCM. [c] PrCN solution containing an excess of Cl$^-$. [d] Reverse oxidation of the radical produced by reduction of [RhCl(CO)(*i*Pr$_2$Ph-bian)] in PrCN at 293 K.

Spectroelectrochemistry in THF. The reversible cathodic behaviour of [RhCl-(CO)(*i*Pr₂Ph-bian)] in THF at room temperature was followed *in situ* by UV-VIS, EPR and IR spectroscopies, in order to collect evidence for the localisation of the unpaired electron in the one-electron-reduced complex predominantly in the lowest π^* orbital of the *i*Pr₂Ph-bian ligand. For additional support, EPR and UV-VIS spectra of the uncoordinated radical anion *i*Pr₂Ph-bian$^{•-}$ were also recorded under the same conditions. The UV-VIS spectral changes accompanying the one-electron reduction of [RhCl(CO)-(*i*Pr₂Ph-bian)] are shown in Fig. 6. Both MLCT bands of the parent complex disappeared. The broad and asymmetric new band arising at 740 nm is attributed to $\pi^*\pi^*$ electronic transitions of the *i*Pr₂Ph-bian$^{•-}$ ligand, consistent with the electronic spectrum of uncoordinated *i*Pr₂Ph-bian$^{•-}$ shown in Fig. 6 (inset). The EPR spectrum of *i*Pr₂Ph-bian$^{•-}$ displays a characteristic quintet arising from the hyperfine splitting by two equivalent ^{14}N nuclei
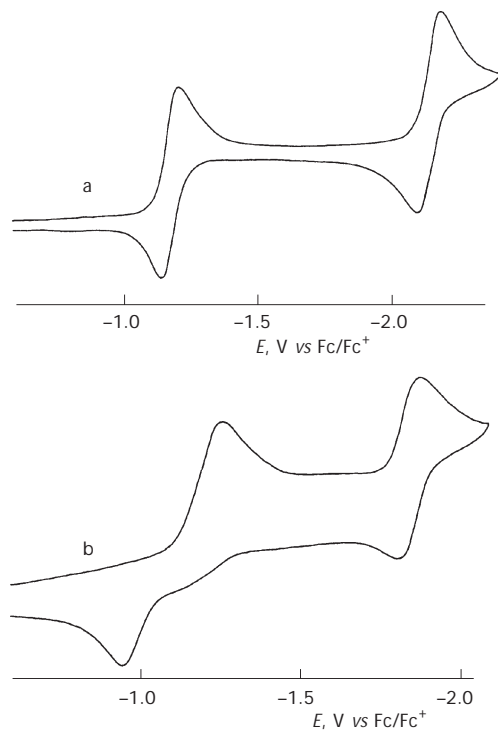
FIG. 4
Cyclic voltammograms of [RhCl(CO)(*i*Pr₂Ph-bian)] in PrCN at T = 218 K (a) and 293 K (b). Conditions: c_{Rh} = 10^{-3} mol dm^{-3}, v = 100 mV s^{-1}, Pt-disk electrode

(99.63% natural abundance, $I = 1$): the value $a_N = 0.23$ mT has been obtained from the simulated signal (Fig. 7a). The similar quintet EPR response of the radical anion [RhCl(CO)(*i*Pr$_2$Ph-bian)]$^{\bullet-}$ ($a_N = 0.26$ mT) is less resolved due to a larger line width caused by unresolved ^{103}Rh and ^{35}Cl/^{37}Cl hyperfine splittings (Fig. 7b).

In the IR ν(CO) region, the conversion of [RhCl(CO)(*i*Pr$_2$Ph-bian)] into the radical anion lowers the CO-stretching frequency by 64 cm^{-1} (Fig. 8, Table I). This fairly large shift, compared to some other redox series based on pseudooctahedral monocarbonyl complexes[29], points to strong trans-influence of reduced *i*Pr$_2$Ph-bian$^{\bullet-}$ on the carbonyl ligand.

Spectroelectrochemistry in PrCN. Differently from THF, where the Rh–Cl bond in [RhCl(CO)(*i*Pr$_2$Ph-bian)]$^{\bullet-}$ remains preserved, the IR spectroelectrochemical experiment in neat PrCN at room temperature gave rise to the formation of a single reduced species absorbing at 1967 cm^{-1} (Fig. 9).
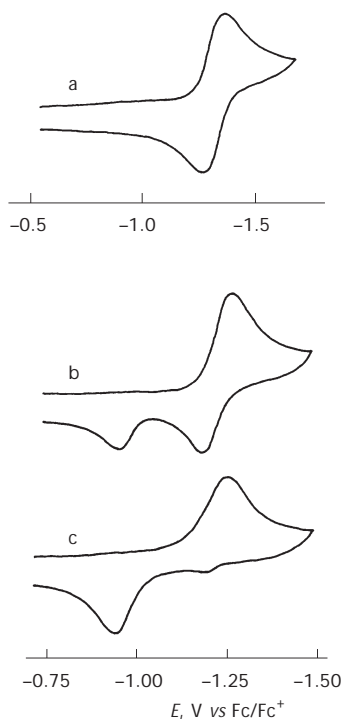

FIG. 5
Cyclic voltammograms of [RhCl(CO)(*i*Pr$_2$Ph-bian)] in neat DCM (a), 30:1 (v/v) DCM/PrCN (b) and 5:1 (v/v) DCM/PrCN (c). Conditions: $c_{Rh} = 10^{-3}$ mol dm^{-3}, $v = 100$ mV s^{-1}, $T = 293$ K, Pt-disk electrode

The EPR spectrum of this radical, recorded in PrCN, shows again a quintet with $a_N = 0.21$ mT. This signal, however, exhibits narrower lines compared to that of [RhCl(CO)(*i*Pr$_2$Ph-bian)]$^{\bullet-}$. With an excess of Cl$^-$ in the PrCN solution, the reduction of [RhCl(CO)(*i*Pr$_2$Ph-bian)] resulted in parallel observation of [RhCl(CO)(*i*Pr$_2$Ph-bian)]$^{\bullet-}$ (ν(CO) at 1930 cm^{-1}) as the major
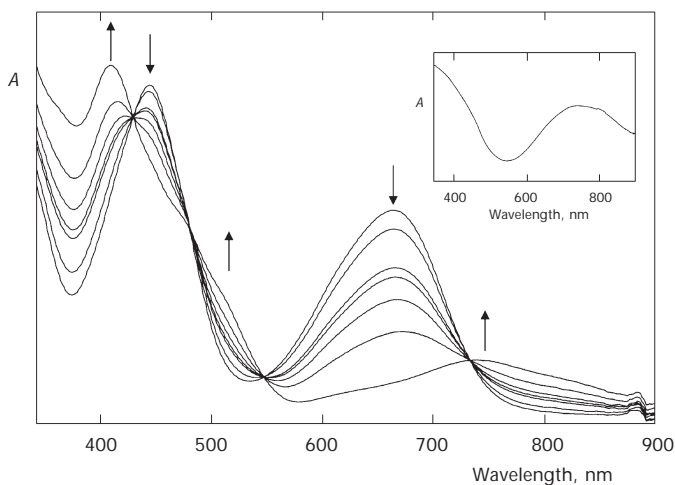
FIG. 6
UV-VIS spectral changes recorded during the reversible reduction of [RhCl(CO)(*i*Pr$_2$Ph-bian)] to the corresponding radical anion in THF at $T = 293$ K, using the new OTTLE cell. Inset: UV-VIS spectrum of the uncoordinated radical anion *i*Pr$_2$Ph-bian$^{\bullet-}$, generated by one-electron reduction of *i*Pr$_2$Ph-bian under the same experimental conditions
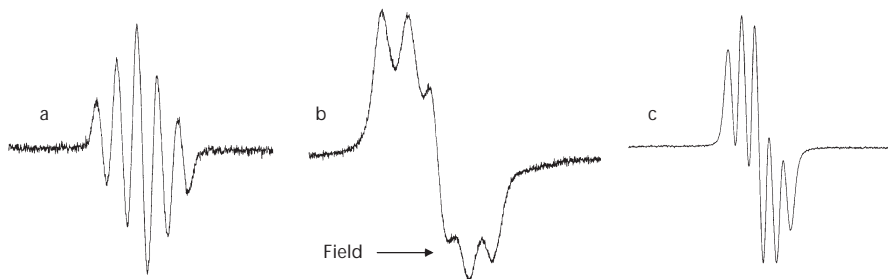
FIG. 7
EPR spectra of uncoordinated *i*Pr$_2$Ph-bian$^{\bullet-}$ in THF at $T = 293$ K (a), [RhCl(CO)(*i*Pr$_2$Ph-bian)]$^{\bullet-}$ in THF at $T = 233$ K (b) and [Rh(CO)(PrCN)(*i*Pr$_2$Ph-bian)]$^{\bullet}$ in PrCN at $T = 293$ K (c). The EPR spectra were recorded *in situ*, using an air-tight EPR spectroelectrochemical cell equipped with a Au-helix working electrode[25]

product and the 1967 cm⁻¹ species. In accordance with the cyclic voltammetric response (see above), the IR and EPR data strongly support the reduction-induced substitution of Cl⁻ with a PrCN molecule and formation of the radical [Rh(CO)(PrCN)(*i*Pr₂Ph-bian)]⁻. This reaction is complete in PrCN but becomes suppressed in the presence of an excess of Cl⁻ or at low
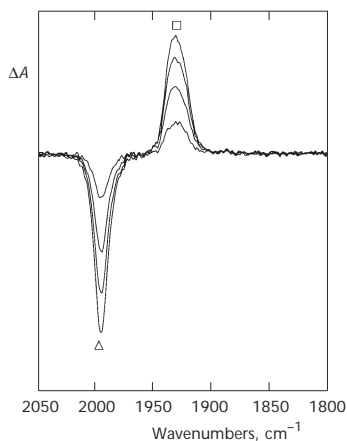

FIG. 8
Difference-absorption IR spectral changes in the CO-stretching region recorded during the reversible reduction of [RhCl(CO)(*i*Pr₂Ph-bian)] (△) to the corresponding radical anion (□) in THF at *T* = 293 K, using the new OTTLE cell
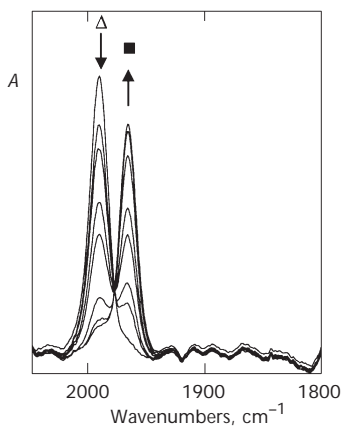

FIG. 9
IR spectral changes in the CO-stretching region recorded during the reduction-induced conversion of [RhCl(CO)(*i*Pr₂Ph-bian)] (△) to the radical [Rh(CO)(PrCN)(*i*Pr₂Ph-bian)]⁻ (■) in PrCN at *T* = 293 K, using the new OTTLE cell

temperatures. At T = 193 K only [RhCl(CO)(iPr$_2$Ph-bian)]$^{•-}$ is observed (Fig. 10). Subsequent one-electron reduction of the radical anion leads to a species absorbing at 1869 cm^{-1}, which can be assigned to the dianion [RhCl(CO)(iPr$_2$Ph-bian)]$^{2-}$, where probably also the second added electron is largely localized on the iPr$_2$Ph-bian ligand. In addition, a minor species is observed at 1904 cm^{-1} (Fig. 10), resulting from a Cl$^-$ substitution reaction of [RhCl(CO)(iPr$_2$Ph-bian)]$^{2-}$ to produce the two-electron-reduced anion [Rh(CO)(PrCN)(iPr$_2$Ph-bian)]$^-$. At T = 218 K, both [RhCl(CO)(iPr$_2$Ph-bian)]$^{•-}$ and [Rh(CO)(PrCN)(iPr$_2$Ph-bian)]$^•$ radical complexes are formed during the first one-electron reduction in similar concentrations. The second one-electron cathodic step at this temperature then promotes the Cl$^-$ substitution to a larger extent than at T = 193 K and [Rh(CO)(PrCN)(iPr$_2$Ph-bian)]$^-$ dominates in the solution over [RhCl(CO)(iPr$_2$Ph-bian)]$^{2-}$ (Fig. 11). The IR spectroelectrochemical experiment performed at room temperature in PrCN containing an excess of Cl$^-$ led to a similar ratio between [Rh(CO)(PrCN)-(iPr$_2$Ph-bian)]$^-$ and [RhCl(CO)(iPr$_2$Ph-bian)]$^{2-}$.

Concluding this part, coordination of the strongly electron-withdrawing iPr$_2$Ph-bian ligand in the [RhCl(CO)(iPr$_2$Ph-bian)] complex results in high stability of the one- and two-electron-reduced products, the radical anion [RhCl(CO)(iPr$_2$Ph-bian)]$^{•-}$ and the dianion [RhCl(CO)(iPr$_2$Ph-bian)]$^{2-}$. The electrons added during the electrochemical reduction reside predominantly in the aromatic π^*(iPr$_2$Ph-bian) system. This conclusion is in full agreement with results of the resonance Raman study (see above) showing that electrons excited with visible light occupy the same orbital system. In strongly coordinating PrCN, the chloride ligand can be substituted by a solvent molecule. The formation of [Rh(CO)(PrCN)(iPr$_2$Ph-bian)]$^•$ and/or [Rh(CO)-(PrCN)(iPr$_2$Ph-bian)]$^-$ can be effectively controlled by temperature variation and/or by the presence of an excess of Cl$^-$ in the PrCN solution. On the other hand, the oxidation of [RhCl(CO)(iPr$_2$Ph-bian)] is irreversible due to the insufficient stabilisation of the Rh(II) oxidation state by the donor ligands. This explanation receives support from the fairly reversible one-electron oxidation observed[30] in the case of the square-planar complex [Rh(Cl)(tpy)] (tpy = 2,2′:6′,2″-terpyridine) with a strongly nucleophilic Rh(I) centre.

Description of the Cryostated OTTLE Cell

The previous version of the cryostated (low-temperature) optically transparent thin-layer electrochemical cell employed for the IR and UV-VIS spectroelectrochemical experiments reported in the preceding section, was de-
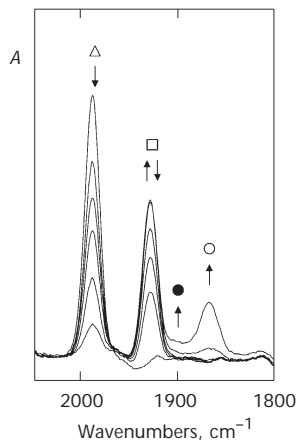
FIG. 10

IR spectral changes in the CO-stretching region recorded during the one-electron reduction of [RhCl(CO)(*i*Pr$_2$Ph-bian)] ($\triangle$) to [RhCl(CO)(*i*Pr$_2$Ph-bian)]$^{\bullet-}$ ($\square$), which further reduces to [RhCl(CO)(*i*Pr$_2$Ph-bian)]$^{2-}$ ($\bigcirc$) and minor [Rh(CO)(PrCN)(*i*Pr$_2$Ph-bian)]$^-$ ($\bullet$), in PrCN at T = 193 K, using the new OTTLE cell
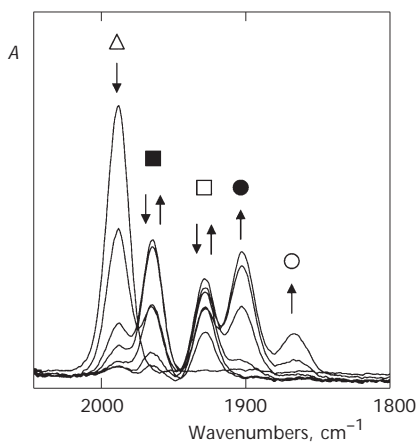

FIG. 11

IR spectral changes in the CO-stretching region recorded during the cathodic transformation of [RhCl(CO)(*i*Pr$_2$Ph-bian)] ($\triangle$) to one-electron-reduced [RhCl(CO)(*i*Pr$_2$Ph-bian)]$^{\bullet-}$ ($\square$) and [Rh(CO)(PrCN)(*i*Pr$_2$Ph-bian)]$^{\bullet}$ ($\blacksquare$) and, successively, to two-electron-reduced [RhCl(CO)-(*i*Pr$_2$Ph-bian)]$^{2-}$ ($\bigcirc$) and [Rh(CO)(PrCN)(*i*Pr$_2$Ph-bian)]$^-$ ($\bullet$), in PrCN at T = 218 K, using the new OTTLE cell

scribed[18] in 1994. Since that time, a number of changes in the successful cell design have been introduced, which improved the cell performance and finally resulted in the construction of the new version, depicted and described in this work. The descriptive part mainly presents new construction features and differences in the cell performance compared to the previous version. Electrochemical characteristics of the cell (thin-layer cyclic voltammetric scans) have been given in the original publication.

The OTTLE cell set-up. Similar to the previous version[18], the complete cell set-up consists of three major parts (Figs 12–14):

a) a home-made double-walled cryostat housing two liquid-N_2 reservoirs, evacuated mantle (with a valve connection to a diffusion pump), heat/cold exchanger with a built-in Pt-100 thermocouple and a throughput for cold N_2 gas streaming at a regulated speed, and an inner cylindrical chamber with crossed pairs of CaF_2 (IR) and quartz (UV-VIS) windows;

b) an inner (low-temperature OTTLE) cell placed into the inner chamber of the cryostat in a close contact with the heat/cold exchanger, which is equipped with built-in heaters and a Pt-100 thermocouple, electrode assemblage in the thin solution layer, filling ports and CaF_2 windows;

c) a microprocessor-driven thermoregulation apparatus DTron 16.1, consisting of a power unit connected to the cell heaters, and a control unit connected to both Pt-100 thermocouples (in the heat/cold exchanger and the inner low-temperature OTTLE cell).

One of the most important construction features of the new cell concerns considerably smaller dimensions and weight reduction, by *ca* 30%, com-

FIG. 12

New low-temperature OTTLE cell. A view of the inner thin-layer cell (left) removed from the cylindrical inner chamber of the cryostat (right)

pared to the original parameters. This facilitates shuttling the cryostat/cell set-up between sample compartments of different spectro(photo)meters in the course of a combined UV-VIS and IR spectroelectrochemical experiment, when mixtures of redox products are analysed at different electrode potential steps or different temperatures. Also the initial cooling period is significantly shortened. The maximum diameter of the cryostat body has been reduced to 12 cm, its maximum height (without the inner low-temperature OTTLE cell) to 43 cm. The dimensions of the copper block housing the thin-layer electrode compartment (Figs 15–17) are, consequently, also smaller: 44 mm diameter, 60 mm height. However, the mass reduction of the inner-cell copper body has not influenced negatively its thermal capacity. Thus, the preselected low temperature of the cell, *e.g.*, 180 K, remains stable for more than 15 min even if the temperature of the heat/cold exchanger, which is set slightly lower, rose by accident above this value owing to empty liquid-N₂ reservoirs.

The cryostat. Apart from the smaller dimensions, the construction of the cryostat (based on Oxford Instruments models) has remained basically unchanged (Figs 12–14). The schematic cross-section view in the previous publication[18], showing the liquid-N₂ reservoirs, nitrogen outlets, heat/cold exchanger with embedded Pt-100 thermocouple, evacuated mantle made of
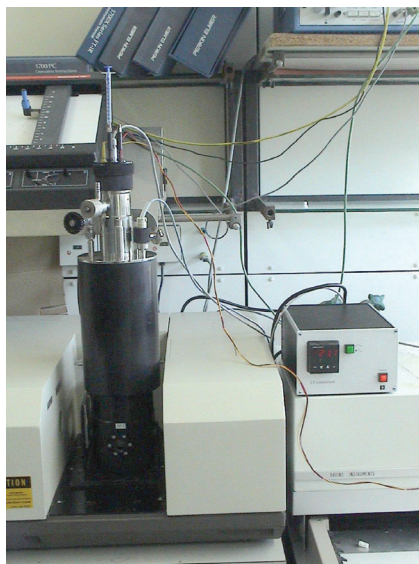

FIG. 13
New low-temperature OTTLE cell. A view of the complete set-up positioned in a sample compartment of an FTIR spectrometer. Right: the thermoregulation unit

FIG. 14
Detailed view of the top part of the cryostat with the thin-layer cell positioned in the inner chamber. Left: connection to diffusion pump (for mantle evacuation) (front) and Pt-100 connector to the thermoregulation apparatus (rear); middle: one of the liquid-N_2 filling ports; right: outlet of N_2 gas from the heat/cold exchanger with the regulation valve (front) and vacuum valve of the inner chamber (rear). On the top of the thin-layer cell are shown the three electrode contacts (front), heater and Pt-100 connector to the thermoregulation apparatus (middle) and the inlet and outlet tubes to the thin solution layer (rear)
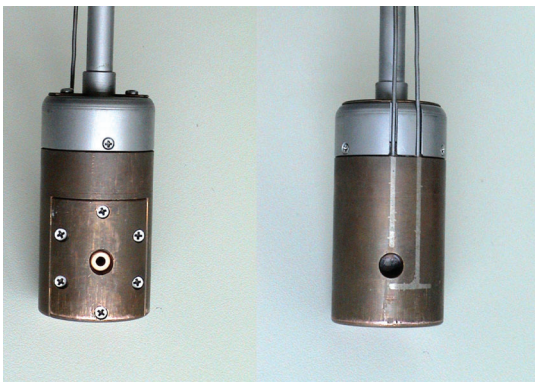

FIG. 15
Detailed view of the front and rear sides of the copper body of the inner thin-layer cell, showing the frontal pressure plate with fixation screws and the soldered air-tight thin-layer filling ports, respectively

anodized aluminium, inner chamber, sealed optical windows, and connection to diffusion pump, is therefore valid also for the new cryostat. Importantly, in the new version, the inner chamber can be evacuated and filled with an overpressure of dry argon or nitrogen gas (to avoid moisture condensation on optical windows) even with the inner thin-layer cell being inserted. The older version was not vacuum-tight and the cell, therefore, had to be placed to the cryostat in a counter-stream of argon.

The inner low-temperature OTTLE cell. The cross-sections of the thin-layer spectroelectrochemical cell are depicted in Figs 16 and 17. Compared with the previous construction, the improvements regard better electronic shielding of the electrode wiring and contacts, and more advanced leakage-proof arrangement of the embedded CaF$_2$ windows. The (masked) Pt (or Au) working (80% transmittance) and Pt auxiliary minigrid electrodes are melt-sealed in the insulating P-E spacer in such a way that they are extended up to the insulated tinned copper leads to the potentiostat; the connecting silver wires in the former version have been avoided due to frequent poor conductivity problems. The surface of the auxiliary electrode has been enlarged. The two CaF$_2$ optical windows (30 mm diameter; purchased from Specac or home-cut from a rod-shaped CaF$_2$ monocrystal) are separated at both sides, from the Cu cell body and a PTFE distance ring, by indium gas-
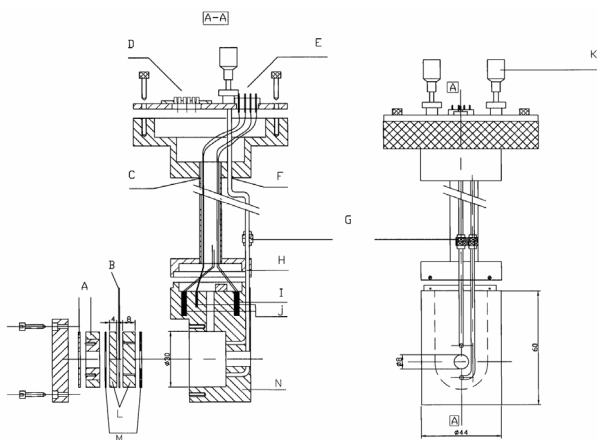

FIG. 16

Details of the inner thin-layer electrochemical cell. Left: cross section; right: side view. (A) Distance PTFE rings. (B) P-E spacer with melt-sealed electrodes. (C, F) Vacuum-tight (soldered) throughputs for the 1/4-inch solution inlet and outlet tubes (H) and for the central hollow tube housing the wiring to electrode plugs (D), Pt-100 thermocouple (I) and heaters (J). (E) Connector plug to the thermoregulation apparatus. (G) Swagelok coupling. (K) Syringe insertion port. (L) CaF$_2$ windows. (M) Indium gaskets

kets, ensuring effective compensation of undesired thermal expansion or contraction. The frontal copper plate for the window fixation is separated from the optical windows by two, thick and thin, PTFE distance rings, employed instead of a single copper one used in the previous version. Further, the pressure at the window surfaces is more regularly divided by using six instead of four fixation screws in the frontal plate (Fig. 15). This arrangement significantly reduces the chance of an accidental crash of the expensive window material. The cell was tested down to 173 K (using PrCN) and proved to be leakage-free at this temperature. The arrangement of the two 40-W heaters and the Pt-100 thermocouple in the copper block (both connected to the thermoregulation unit) does deviate from that in the previous cell version. Due to a better electronic shielding of the electrode contacts, the response of the OTTLE cell during electrolyses is nearly noiseless. Only the regular heating periods of a few seconds duration, controlled by the thermoregulation set-up, are registered by the potentiostat circuit.

Thermoregulation apparatus. The temperature control in the previous version of the low-temperature OTTLE cell was achieved with the same thermoregulation unit (Cryoson) as adapted in our laboratory nearly two decades ago for a special cryogenic (liquid-Xe/Kr) cell[31]. In the new cell version, the temperature control is carried out with a small-dimensional apparatus DTron 16.1 equipped with a microprocessor (see Fig. 13). The con-
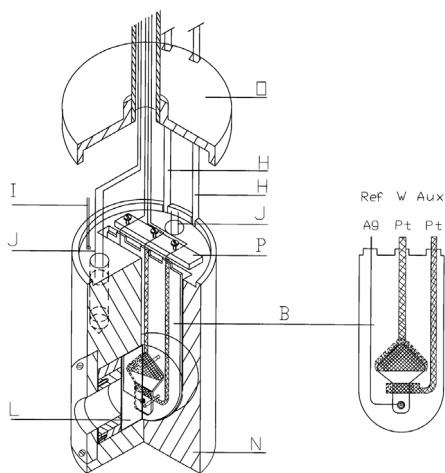

Fig. 17
Details of the inner thin-layer electrochemical cell, showing the position of the P-E spacer (thickness of *ca* 0.2 mm) with the melt-sealed three-electrode system (B). (I), (J), (L) – see Fig. 16. (N) Cylindrical copper block. (O) Upper cover plate. (P) Insulating PTFE plate

struction of DTron 16.1 (Scheme 1) basically derives from the original concept (Jumo, Germany), with an adaptation of the power unit electronics to the different heating elements embedded in the low-temperature OTTLE cell body (Figs 16 and 17). These elements are two 24-V low-ohmic resistors; for fast temperature rise the voltage can be increased to 40 V. The heating function is controlled in a precise and trouble-free way by an electronic relay. The temperature is measured by the control unit connected to two Pt-100 thermocouples, one placed close to the thin solution layer of the inner low-temperature cell and the other in the heat/cold exchanger. Both temperatures can be read independently, with a precision of 0.1 K, on a switchable digital display. The temperature variation between the heating and cooling periods does not exceed 0.5 K. The thermoregulation was tested with very satisfactory results in the course of spectroelectrochemical experiments performed at temperatures down to 173 K.

In summary, the new, user-friendly version of the low-temperature OTTLE spectroelectrochemical cell has proved to be a very convenient tool for temperature-dependent mechanistic redox studies and for characterisation of thermally unstable transient redox products in the UV-VIS-NIR-IR region. In this work the reliable cell performance has been demonstrated on the example of the reduction of [RhCl(CO)(*i*Pr₂Ph-bian)] in PrCN at 218 and 193 K. Another recent example of the cell application can be found in the literature[32]. In addition, the cell can also be adapted for (resonance) Raman studies at low temperatures, using appropriate optics for the collection of laser light back-scattered in the close vicinity of the working electrode.
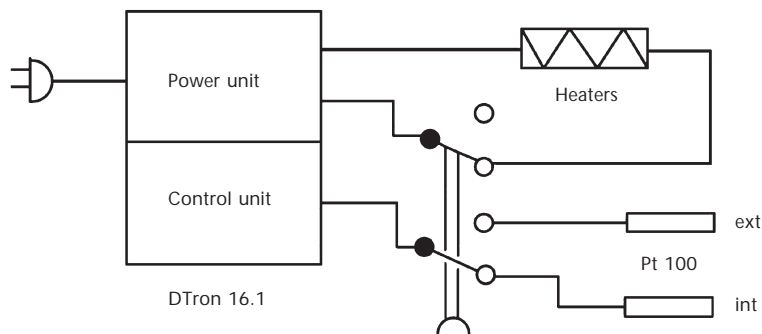
SCHEME 1
Schematic representation of the thermoregulation apparatus DTron 16.1

REFERENCES

1. a) Gonsalvi L., Gaunt J. A., Adams H., Castro A., Sunley G. J., Haynes A.: *Organometallics* **2003**, *22*, 1047; b) Aresta M., Quaranta E.: *J. Organomet. Chem.* **1993**, *463*, 215, and references therein; c) Garcia V., Garralda M. A., Ibarlucea L.: *Trans. Met. Chem. (London)* **1985**, *10*, 288; d) Clauti G., Zassinovich G., Mestroni G.: *Inorg. Chim. Acta* **1986**, *112*, 103; e) Pruchnik V., Wajda K.: *J. Organomet. Chem.* **1979**, *164*, 71; f) Zassinovich G., Camus A., Mestroni G.: *J. Organomet. Chem.* **1977**, *133*, 377; g) Zassinovich G., Mestroni G., Camus A.: *J. Organomet. Chem.* **1977**, *91*, 379; h) Gillard R. D., Harrison K., Mather I. H.: *J. Chem. Soc., Dalton Trans*. **1975**, 133; i) Mestroni G., Camus A., Zassinovich G.: *J. Organomet. Chem.* **1974**, *65*, 119; j) Cocevar C., Mestroni G., Camus A.: *J. Organomet. Chem.* **1972**, *35*, 389; k) Lawson D. N., Wilkinson G.: *J. Chem. Soc.* **1965**, 1900; l) Chatt V., Venanzi L.: *J. Chem. Soc*. **1957**, 4735; m) Mitryaikina M. A., Gracheva L. S., Polovnyak V. K., Usachev A. E., Yablokov Yu. V.: *J. Gen. Chem. U.S.S.R.* **1992**, *62*, 1992.
2. a) Botteghi C., Paganelli S.: *J. Organomet. Chem.* **1993**, *451*, C18; b) Bayón J. C., Esteban P., Real J.: *J. Organomet. Chem.* **1991**, *403*, 393; c) Saus A., Nhu Phu T., Mirbach M. J., Mirbach F. M.: *J. Mol. Catal*. **1983**, *18*, 117; d) Markó L.: *Aspects of Homogeneous Catalysis*, Vol. 2. D. Reidel Publishing Co., Dordrecht 1974.
3. Brockmann M., tom Dieck H., Klaus J.: *J. Organomet. Chem.* **1986**, *301*, 209.
4. a) Zassinovich G., Mestroni G., Camus A.: *J. Mol. Catal.* **1987**, *42*, 81; b) Zassinovich G., Mestroni G., Camus A.: *J. Mol. Catal.* **1977**, *2*, 63; c) Mestroni G., Zassinovich G., Camus A.: *J. Organomet. Chem*. **1977**, *140*, 63; d) Zassinovich G., Mestroni G., Camus A.: *Inorg. Nucl. Chem. Lett.* **1976**, *12*, 865; e) Pasternak H., Pruchnik F.: *Inorg. Nucl. Chem. Lett.* **1976**, *12*, 591; f) Pasternak H., Glowiak T., Pruchnik F.: *Inorg. Chim. Acta* **1976**, *19*, 11.
5. Bolinger C. M., Story N., Sullivan B. P., Meyer T. J.: *Inorg. Chem*. **1988**, *27*, 4582.
6. Morton S., Nixon J. F.: *J. Organomet. Chem.* **1985**, *282*, 123.
7. van Slageren J., Vermeer A. L., Stufkens D. J., Lutz M., Spek A. L.: *J. Organomet. Chem.* **2001**, *626*, 118.
8. Deeming A. J., Rothwell I. P., Hursthouse M. B., Malik K. M. A.: *J. Chem. Soc*. **1979**, 1899.
9. van der Poel H., van Koten G., Vrieze K.: *Inorg. Chim. Acta* **1981**, *51*, 241.
10. van der Poel H., van Koten G., Vrieze K.: *Inorg. Chim. Acta* **1981**, *51*, 253.
11. tom Dieck H., Klaus J.: *J. Organomet. Chem*. **1983**, *246*, 301.
12. Delgado-Laita E., Sanchez-Muñoyerro E.: *Polyhedron* **1984**, *3*, 799.
13. Varshavskii Y. S., Kiseleva N. V., Buzina N.: *Zh. Neorg. Khim.* **1971**, *16*, 863.
14. Crociani B., Di Bianca F., Paci M., Boschi T.: *Inorg. Chim. Acta* **1988**, *145*, 253.
15. van Asselt R., Rijnberg E., Elsevier C. J.: *Organometallics* **1994**, *13*, 706.
16. van Asselt R., Elsevier C. J., Smeets W. J. J., Spek A. L.: *Inorg. Chem.* **1994**, *33*, 1521.
17. Rossenaar B. D., Hartl F., Stufkens D. J.: *Inorg. Chem.* **1996**, *35*, 6194.
18. Hartl F., Luyten H., Nieuwenhuis H. A., Schoemaker G. C.: *Appl. Spectrosc.* **1994**, *48*, 1522.

19. van Asselt R., Elsevier C. J., Smeets W. J. J., Spek A. L., Benedix R.: *Rec. Trav. Chim. Pays-Bas* **1994**, *113*, 88.

20. Dova E., Goubitz K., van Langevelde A., Driessen R., Mahabiersing T., Blaauw R., Peschar R., Schenk H.: *J. Synchrotron Rad.* **2001**, *8*, 1186.

21. Hartl F., Goubitz K., Fraanje J., Mahabiersing T.: Unpublished results.

22. Duling D.: *Public EPR Software Tools*. National Institute of Environmental Health Sciences; http://epr.niehs.nih.gov/pest.html.

23. Gritzner G., Kůta J.: *Pure Appl. Chem.* **1984**, *56*, 461.

24. Pavlishchuk V. V., Addison A. W.: *Inorg. Chim. Acta* **2000**, *298*, 97.

25. Hartl F., Groenestein R. P., Mahabiersing T.: *Collect. Czech. Chem. Commun.* **2001**, *66*, 52.

26. van Slageren J., Klein A., Záliš S., Stufkens D. J.: *Coord. Chem. Rev.* **2001**, *219–221*, 937.

27. Mašková E., Vlček A., Jr.: *Inorg. Chim. Acta* **1996**, *242*, 17.

28. Záliš S., Farrell I. R., Vlček A., Jr.: *J. Am. Chem. Soc.* **200**3, *125*, 4580.

29. Chardon-Noblat S., Da Costa P., Deronzier A., Mahabiersing T., Hartl F.: *Eur. J. Inorg. Chem.* **2002**, 2850.

30. a) de Pater B. C.: *Ph.D. Thesis*. University of Amsterdam, Amsterdam 2003; b) de Pater B. C., Frühauf H.-W., Vrieze K., Budzelaar P. H. M., Gal A. W., de Gelder R., Baerends E. J., McCormack D., Lutz M., Spek A. L., Hartl F.: *Eur. J. Inorg. Chem.*, submitted.

31. Andréa R. R., Luyten H., Vuurman H. H., Stufkens D. J., Oskam A.: *Appl. Spectrosc.* **1986**, *40*, 1184.

32. Hoshino Y., Higuchi S., Fiedler J., Su Ch.-Y., Knödler A., Schwederski B., Sarkar B., Hartmann H., Kaim W.: *Angew. Chem.* **2003**, *42*, 674.